

Contents lists available at ScienceDirect

Nano Energy

journal homepage: www.elsevier.com/locate/nanoen





Graphene-supported single atom catalysts for high performance lithium-oxygen batteries

Hoilun Wong ^a, Tongchao Liu ^b, Mohsen Tamtaji ^a, Xiaozhou Huang ^b, Tsz Wing Tang ^a, Md Delowar Hossain ^a, Jun Wang ^a, Yuting Cai ^a, Zhenjing Liu ^a, Hongwei Liu ^a, Khalil Amine ^b, William A. Goddard III ^{c,*}, Zhengtang Luo ^{a,d,**}

- ^a Department of Chemical and Biological Engineering and William Mong Institute of Nano Science and Technology, Hong Kong University of Science and Technology, Clear Water Bay, Kowloon, Hong Kong
- ^b Chemical Sciences and Engineering Division Argonne National Laboratory, 9700 Cass Ave, Lemont, IL 60439, USA
- ^c Materials and Process Simulation Center (MSC), California Institute of Technology, MC 139-74, Pasadena, CA 91125, USA

ARTICLE INFO

Keywords: Single atom catalysts Density functional theory Oxygen reduction reaction Oxygen evolution reaction Overpotentials Machine learning

ABSTRACT

The optimal choice of d-block metals in single atom catalysts (SACs) is crucial for designing efficient electrocatalysts for activating the Oxygen reduction reaction (ORR)/ Oxygen evolution reaction (OER) in lithium-oxygen batteries (LOBs). Herein, we used the Quantum Mechanics methods to understand the origin of reactivity for a series of 16 d-block metals supported on nitrogen-doped graphene as SACs for ORR and OER in LOBs. Based on the Gibbs free energy calculations, we found that among the 16 SACs investigated, Zn-SAC exhibits the highest electrochemical activity with the lowest overpotential of 0.17 V. We then used machine learning (ML) to develop an intrinsic descriptor, Φ , that correlates the catalytic activity with electronic and chemical properties of the catalytic centers at the M-N₄ active site on graphene surface. We established a linear relationship between Φ and the catalytic activity that provides guidance for designing efficient SACs for electrocatalysis in LOBs. To validate these predictions, we report electrochemical measurements showing that Zn-SAC exhibits an ultra-stable cyclability with reduced overpotentials over Mo-SAC and nitrogen-doped graphene (NG), confirming our theoretical prediction. This fundamental work provides a deep understanding on the rational design of efficient SACs for OER/ ORR in LOBs.

1. Introduction

Aprotic lithium-oxygen batteries (LOBs) have been considered as a next-generation battery technologies, due to its ultrahigh theoretical energy density (\sim 3600 Wh kg $^{-1}$), 5–10 times higher than the state-of-the-art lithium-ion batteries (LIBs), to support the development of electric vehicles (EVs). [1] Nonaqueous LOBs typically consist of lithium metal anode, separator, Li ionic conducting electrolyte, and a perforated carbon cathode, allowing access of O₂. [2,3] During discharging, O₂ is first adsorbed at the cathode surface and then reduced to superoxide (O₂), combining with Li $^+$ to form lithium superoxide (LiO₂). This intermediate is thermally unstable and is further reduced easily to lithium peroxide (Li₂O₂) via two possible routes:

However, this battery system suffers from poor cyclability, low round-trip efficiency and inferior rate capability, which mainly originate from the chemical inertness of oxygen gas and the poor electrical conductivity of lithium peroxide (Li_2O_2). This leads to sluggish kinetics for the ORR and the OER. [5–7] In response to these challenges, developing a highly efficient catalyst at the cathode is vital to boost the reaction rate and reduce the reaction overpotentials. Extensive research effort has been devoted to designing efficient catalysts, such as, carbonaceous materials [8–12], noble metals [13–16] and metal alloys [17,18], transition metal oxides and sulfides [19–22]. However, these materials

E-mail addresses: wag@caltech.edu (W.A. Goddard), keztluo@ust.hk (Z. Luo).

d Hong Kong University of Science and Technology-Shenzhen Research Institute, No. 9 Yuexing first RD, Hi-Tech Park, Nanshan, Shenzhen 518057, China

⁽¹⁾ Disproportionation: $2\text{LiO}_2 \rightarrow \text{Li}_2\text{O}_2 + \text{O}_2$

⁽²⁾ Electrochemical reduction: $LiO_2 + Li^+ \rightarrow Li_2O_2$. [4]

^{*} Corresponding author.

^{**} Corresponding author at: Department of Chemical and Biological Engineering and William Mong Institute of Nano Science and Technology, Hong Kong University of Science and Technology, Clear Water Bay, Kowloon, Hong Kong.

still face shortcomings, including high cost and active site passivation by the insulating Li_2O_2 .

Heterogeneous single-atom catalysts (SACs) on solid supports are emerging as a new frontier in electrocatalysis. By downsizing the catalyst metal particles or clusters, single-atom catalysts merit the advantages of typical homogeneous and heterogenous catalysts, with improved catalytic activity and full metal utilization. This simultaneously reduces the consumption of precious metal resources and the costs, while retaining the advantages of high stability and reusability of heterogeneous catalysts. [23-25] In addition, the homogeneity of the active sites makes the single-atom catalyst highly selective towards specific products. [26] At the atomic level, the tunable coordination environment around the single atom provides catalyst uniqueness in activity, selectivity, durability, and electronic structure. The electron confinement from the quantum size effect gives the catalyst a distinctive energy gap between the highest occupied molecular orbital (HOMO) and the lowest unoccupied molecular orbital (LUMO) and a discrete energy level distribution, facilitating charge transfer. Nevertheless, due to the increased surface free energy, the metals at SAC are prone to agglomeration, therefore, bulk metals and metal oxides are typical supports to stabilize the catalyst structure. Unfortunately, most of these substrates are insulators or semiconductors, which may be very unstable under such harsh electrochemical operation conditions, strong acid or base. Carbon supports, especially graphene, becomes a promising alternative since they provide high surface area, superior electrical conductivity, and good stability. [27] In addition, the bond strength between the single metal atom and the substrate can be enhanced by adding electron rich components (i.e. nitrogen doping) and creating defects to avoid the metal atom aggregation. [28] Most recently, it has been reported that single atom catalysts of Ru [29] and Co [30,31] on nitrogen doped carbon substrate play a critical role in reducing the reaction overpotential for the ORR/ OER processes, leading to high specific capacity and excellent cycling stability in LOBs. However, the origin of this activity remains unclear for d-block metals on graphene support. Moreover, the relationships of metal properties and catalyst structures to catalytic activities have not yet been established for designing efficient SACs for ORR/ OER in LOBs.

Herein, we utilized quantum mechanical calculations (density functional theory, DFT) to predict the catalytic activities of 16 different d-block metal single atoms embedded to the nitrogen doped sites of a graphene support. We found that Zn-SAC exhibits the highest ORR/OER activities. These studies found that the Zn-N₄ catalytic center binds with LiO₂ only weakly, reducing the reaction overpotential to enhance the reaction rate and stability of the catalyst. We find that the activity of SACs correlates highly with the Gibbs free energy of the adsorbed LiO₂. In order to provide guidance for designing effective SACs for ORR/OER we used the supervised machine learning (ML) method to develop a descriptor, Φ . That is based on the metal properties as electronegativity (EN), enthalpy of vaporization (EV), atomic radius (r_{atomic}) and number of electrons in d-orbital ($N_{e,d-orbital}$).

Guided by these predictions, we synthesized two types of SACs,

- Zinc (Zn-SAC) and
- Molybdenum (Mo-SAC),

both embedded in the N-doped graphene surface. We then characterized the atomic coordination and structure experimentally using X-ray absorption fine structure (XAFS) and the direct imaging from scanned transmission electron microscope (STEM). We identified the presence of M-N₄ moieties and confirmed the high loading and uniform distribution of metal atoms on the graphene surface. We compared the electrochemical performance of Zn-SAC with that of Mo-SAC and NG and found that Zn-SAC enabled a more stable cycling performance with lower overpotential, in good agreement with our theoretically derived linear activity- $G_{\rm LiO2}$ trend. This work provides systematic guidance for designing highly efficient SAC for LOBs while providing fundamental

insights in how to choose the optimum metal for the ORR/ OER application.

2. Computational results and discussion

To understand in-depth the redox kinetics and thermodynamics of SACs needed for improving the performance of ORR/ OER in LOBs, we carried out DFT calculations to predict the overpotentials from the free energy diagram, based on the Nørskov method. In this study, we considered three elementary reaction steps [31–33] as.

(a) 4 (Li⁺ + e⁻) + 2
$$O_2$$
 + * \rightarrow Li O_2 * + 3 (Li⁺ + e⁻) + O_2 ,
(b) Li O_2 * + 3 (Li⁺ + e⁻) + O_2 \rightarrow Li $_2$ O $_2$ * + 2 (Li⁺ + e⁻) + O_2 ,
(c) Li $_2$ O $_2$ * + 2 (Li⁺ + e⁻) + O_2 \rightarrow Li $_4$ O $_4$ *.

The overpotential (η) is used to describe quantitatively the catalytic activity of the SACs. It is calculated between the limiting potentials and the equilibrium potential (U_{eq}). The limiting potentials include the discharge potential, U_{DC} , the highest potential to make all intermediate steps in ORR process downhill and the charge potential, U_C , the lowest voltage to shift all intermediate steps in OER process to also be downhill. The discharge overpotential (η_{ORR}) and charge potential (η_{OER}) are expressed as Eqs. (1) and (2), respectively:

$$\eta_{ORR} = U_{eq} - U_{DC} \tag{1}$$

$$\eta_{OER} = U_C - U_{eq} \tag{2}$$

The equilibrium potential (U_{eq}) is defined as the voltage that can drive the ORR/ OER to occur spontaneously with zero reaction free energy, calculated from the Nernst equation:

$$U_{eq} = -\Delta G_f / n \tag{3}$$

where ΔG_f is the total Gibbs free energy change of the reaction (calculated by deducting the free energy of Li and O₂ from the total free energy of Li₄O₄, as described in Eq. (2) in supplementary information), n is the number of electrons involved in the redox reactions, (which is 4 in our study), and e is the elementary charge.

In the SAC structure (Fig. 1a), a metal atom is bonded with 4 nitrogen atoms supported on the planar carbon substrate. It has been reported experimentally and theoretically that the metal and whether it is bonded to nitrogen or carbon atoms can affect the catalysts activity for electrochemical reactions. The nitrogen and carbon atoms in the substrate of SACs are considered as non-metal sites. Therefore, we constructed a molecular model of SACs with all possible non-metal active sites, namely, graphitic C, graphitic N, pyridinic 3 N, pyridinic 4 N and pyrrolic N, to understand the substrate activity towards ORR/OER. Fig. 1b shows the free energy diagram for the pyridinic 4 N substrate as example. The inset figure at the bottom shows the energetically optimized adsorption structure of intermediates along the reaction pathway. At zero potential (U=0), the energy difference between each step accounts for the adsorption energies. Because N is more electronegative than C, electrons are more likely to accumulate around the N atom than the carbon rings in the structure. Therefore, at the active sites of pyrrolic N, pyridinic 3 N and pyridinic 4 N, the δ^+ lithium atoms of LiO₂ and Li₂O₂ tend to be coordinated with N atoms, with a strong interaction. In comparison to graphitic C and graphitic N, the LiO2 and Li2O2 adsorption are weak, which has a strong influence on the decomposition behavior of Li₂O₂ and Li₄O₄. This leads to smaller overpotentials, as presented in Fig. 1c, in agreement with previous literature. [34,35] Based on the free energy diagrams in Fig. 1b and S1a-d, in Supporting Information, the overall overpotentials increase in the sequence of Graphitic N (0.93 V) < Graphitic C (1.02 V) < Pyridinic 3 N (1.82 V) < Pyrrolic N (2.66 V) < Pyridinic 4 N (2.71 V).

Functionalizing graphene with a single metal atom SAC provides a single active site for the catalytic reaction as illustrated in Fig. 1d. The molecular model with a d-block metal atom embedded in graphene but surrounded by four nitrogen atoms, can form strong covalent bonds to

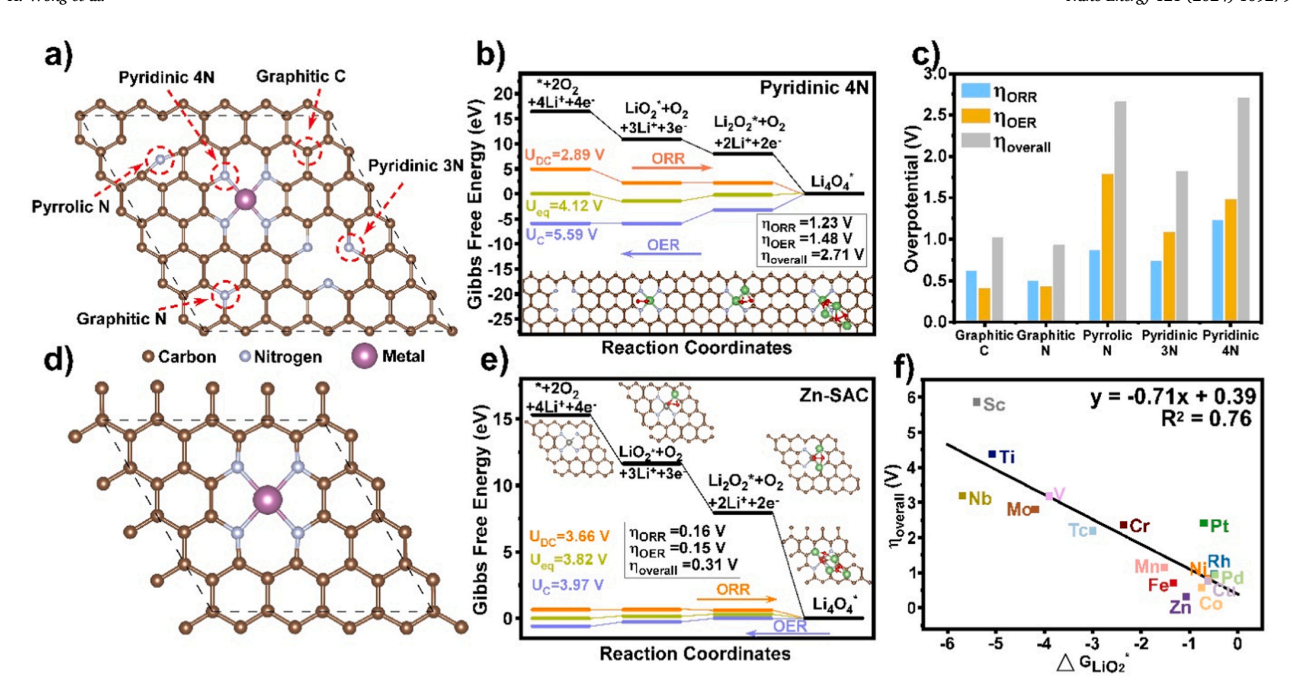


Fig. 1. Proposed molecular models of single atom catalyst and the Gibbs free energy calculations for ORR/ OER. (a) Illustration of all possible reaction sites in the nitrogen doped graphene, not bonded to metal. (b) Gibbs free energy diagram for both ORR/ OER paths with the reaction site of pyridinic 4 N. (c) Comparison of the discharge, charge and overall overpotentials towards all the non-metallic reaction sites. (d) Metal active site coordinated with four nitrogen atoms in graphene substrate. (e) Gibbs free energy diagram of zinc single atom catalyst (Zn-SAC) for ORR/OER. (f) Correlations between the calculated overall overpotentials and the Gibbs free energy of LiO₂ (ΔG_{LiO_3} .).

create hybrid electronic properties, which potentially could induce ORR/ OER catalytic activity. Gibbs free energy studies were performed with various metals SAC with some exhibiting activity towards ORR/ OER for LOBs. Among them,

- the lowest overpotential is achieved on Zn-SAC (0.31 V),
- followed by Co-SAC (0.57 V),
- while Sc-SAC (5.86 V) delivered the highest overall overpotentials.

We applied the DFT+U method to the Gibbs free energy calculation, the results in Table S2 and Fig. S2, Supporting Information found insignificant differences between the DFT and DFT+U. Fig. 1e and S3a in supporting information show that for ORR, the rate determining step (RDS) for Zn-SAC and Co-SAC is formation of LiO2, while the RDS for Sc-SAC (Fig. S3b, Supporting Information) is formation of Li_2O_2 . In the OER process, the RDS for Zn-SAC and Co-SAC is decomposition of Li₄O₄, while the RDS for Sc-SAC is oxidation of LiO2. We found that the catalytic activity of SACs correlates linearly with the Gibbs free energy of LiO_2 (ΔG_{LiO_2}), as shown in Fig. 1f. Zn-SAC has a very weak interaction with LiO₂ leading to a low Gibbs free energy ($\Delta G_{LiO2} = -1.07$ eV), while Sc-SAC, Ti-SAC, Nb-SAC and V-SAC exhibited highly negative Gibbs free energy (-5.39, -5.07, -5.69 and -3.90 eV, respectively), indicating strong interaction with LiO2. This high LiO2 adsorption energy makes the LiO2 reduction to form Li2O2 unfavorable, leading to higher discharge overpotential. In contrast, a smaller adsorption energy makes it easier for LiO2 to form Li2O2 by chemical disproportionation, in which large Li₂O₂ toroid are more likely generated rather than large thin-films, contributing to high discharge capacity as dissolution of LiO2 in the electrolyte releases more active catalyst surface for cathode reactions. Compared with the non-metal sites in SACs, most of the single metal atoms, apart from, Sc, Ti, V, Nb and Mo in the M-N₄ moieties enhance the activity towards ORR/ OER process, highlighting the role of single metal in reducing the reaction overpotentials for LOBs.

Machine Learning (ML) was applied as an instrument to establish a

good structure-activity relationship for predicting overpotential and to examine feature importance analysis to help toward the accelerated design of SACs. [36–38] In order to do this, we used Support Vector Regression (SVR) as a supervised ML algorithm with the radius basis function (rbf) kernel and hyperparameters of C=10 and gamma= 1. The input data (17 data points) was split into the training data (80%, 13 data points) and test data (20%, 4 data points). The input features include the atomic radius, atomic weight, atomic number, period number, group number, electronegativity (EN), ionization energy, electron affinity, enthalpy of vaporization (EV), covalent radius, number of valence electron, isolated electron in d orbital and d-band center of the metal centered in SAC structure.

Fig. 2a displays the parity plot of ML- versus DFT-predicted overpotentials for SACs indicating acceptable MSE values of 0.26 eV² and 0.29 eV² with R² values of 0.952 and 0.998 for the training and test data, respectively, without the signs of unfitting. Moreover, the feature importance analysis on the overpotentials was performed based on the permutation method and displayed in Fig. 2b. This indicates that the descriptors of electronegativity, total electrons in d orbitals, unpaired electrons in d orbital, ionization energy, covalent radius, and group number of metal atoms show a reasonable feature importance. Particularly, Fig. 2b indicates that the new Φ descriptor is appropriate based on its higher feature importance. We find that the total number of d electrons (θ d) and electronegativity (EN) of metal atom are the other most significant and interpretable parameters, conforming to the previous works. [36] Indeed, increasing the d electrons and electronegativity of metal atoms, directly affects the binding strength of reaction intermediates, which in turn affects the reaction overpotential.

Based on these results, we developed a new descriptor, Φ to predict the SAC activity for ORR/ OER of LOBs that is comprised of the input features of EN, EV, r_{atomic} and $N_{e.d-orbital}$ of the central metals in SACs:

$$\Phi = (EN \times EV)/(r_{atomic} \times N_{e,d-orbital}).$$

To explore this activity relation, we plotted the activity descriptor

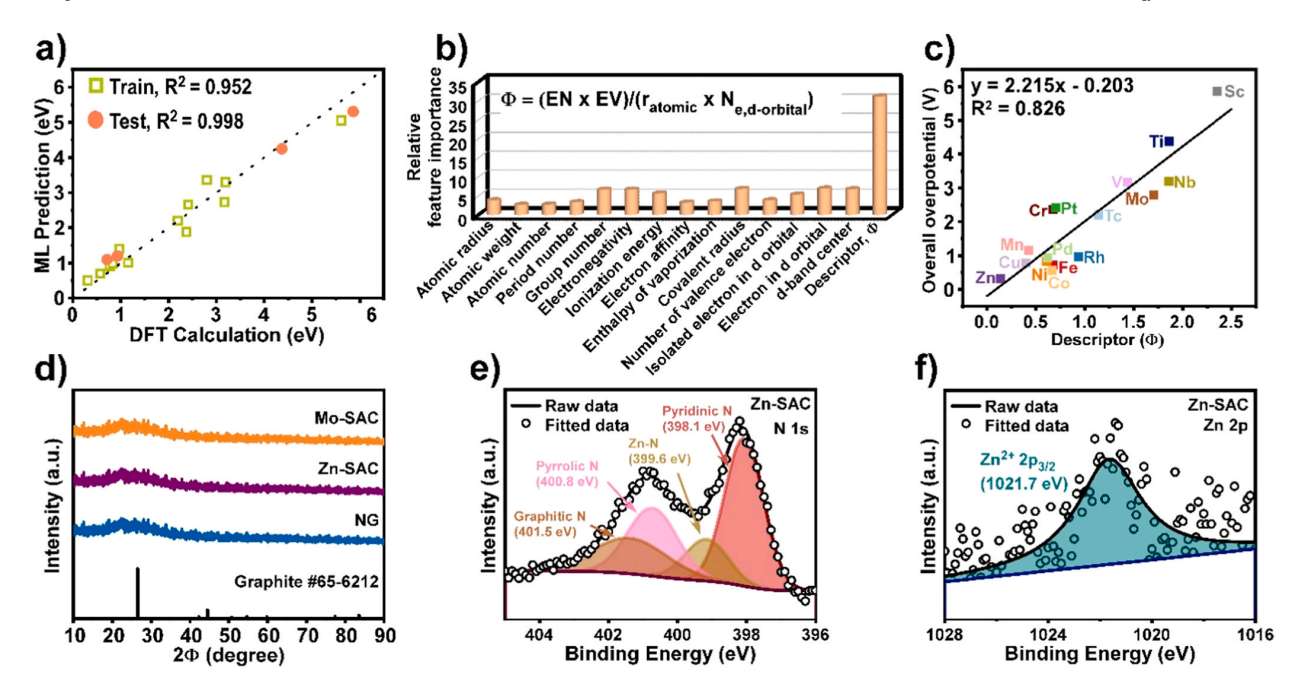


Fig. 2. Relation between the SAC descriptor (Φ) and activity in ORR/ OER based on the DFT-trained machine learning for chemical composition of single atom catalysts. (a) Comparison of the of DFT-calculated and machine learning predicted $\eta_{overall}$. (b) The importance of various features in SACs for ORR/ OER. (c) Overall overpotential based on the Φ descriptor for SACs, showing an inversely linear relationship. (d) XRD patterns of Mo-SAC, Zn-SAC, and NG. (e, f) High-resolution XPS spectra of N 1 s and Zn 2p.

against the corresponding value of Gibbs free energies of LiO_2 for all SACs (Fig. 2c), finding a good linear correlation with $\eta_{overall}$. The overall overpotential decreases with the decreasing Φ . This implies that the decreased tendency of the metal atom to attract the electrons, the less energy required for vaporization, a larger atomic radius, and a larger number of electrons in d-orbitals tend to reduce the overpotential for ORR/ OER in LOBs. This Φ works well to predict the catalytic performance for SACs, providing guidance for designing efficient catalyst for LOBs.

3. Experimental validation and discussion

Based on the theoretical analysis described above, we synthesized two kinds of SACs (Zn and Mo) using graphene oxide (GO) as the substrate, acrylamide as the nitrogen precursor and metallic salts (details in the Experimental Section), according to the methods developed in our group. [39,40] Sc-SAC performed the worst in our calculation results, because of the strong interaction with LiO2, as shown in Fig. 1f. The crystalline structure of Zn-SAC and Mo-SAC were characterized by X-ray crystallography (XRD) in Fig. 2d. For the three samples of Zn-SAC, Mo-SAC and NG, a broad peak was observed at ~ 23°, attributed to the (002) lattice planes of graphite while no distinct peaks are found from the presence of metal crystals in the composite sample, indicating single atom dispersion. In addition, the full X-ray photoelectron spectroscopy (XPS) spectra of Zn-SAC and Mo-SAC (Fig. S4, Supporting Information) confirms the elemental composition of Zn, Mo, N, C and O in the as-prepared SACs samples. The high-resolution N 1 s spectrum in Fig. 2e identifies three types of nitrogen active sites in Zn-SAC at binding energies of 398.1, 400.8 and 401.5 eV, corresponding to pyridinic N, pyrrolic N, and graphitic N, respectively. [41,42] Moreover, the deconvoluted Zn-N (399.6 eV) reveals the existence of Zn-N sites in Zn-SAC. To further verify the presence of Zn-Nx, the Zn 2p spectrum was obtained (Fig. 2f). A peak at 1021.7 eV was identified, corresponding to the Zn^{2+} 2p_{3/2} electronic states, but not associated with Zn-O (1022 eV), showing that only Zn-N_x exists in the composite, with no ZnO. [43]

Similarly, for Mo-SAC, the pyridinic N, pyrrolic N and graphitic N were fitted at 398.2, 400.6 and 401.8 eV, respectively((Fig. S5a, Supporting Information), while the peak at 396.6 eV was observed, corresponding to the N-Mo bonds (Fig. S5b, Supporting Information). [44].

The atomic structure of the SAC was characterized by annular darkfield scanning transmission electron microscopy (ADF-STEM). Fig. 3a and Fig. S6a in Supporting Information shows the low-magnification STEM images of the Zn-SAC and Mo-SAC, respectively, indicating the 2D structure of ultrathin graphene substrate. The high-resolution STEM image in Fig. 3b, clearly demonstrates a clean carbon film without no nanoparticles and impurities observed on the surface, which confirms that no metal atoms aggregated during the material synthesis. In addition, the amorphous structure of Zn-SAC shown in Fig. 3c comes from the carbon materials, indicating no formation of nanoparticles in the composite. Fig. 3d, e displays the uniform distribution of the atomically isolated Zn atoms (brighter dots circled in red) on the whole graphene nanosheet. Similarly, atomically dispersed Mo atoms are detected uniformly throughout the graphene substrate in Fig. S6b, Supporting Information. Furthermore, the energy dispersive analysis (EDS) mapping images in Fig. 3f and Fig. S7, Supporting Information confirms the existence of C, N, Zn and Mo and the homogeneous dispersion of the atoms within the entire carbon scaffold.

To explore the chemical state and atomic coordination environment of SAC structures, XAFS measurements were carried out, as shown in Fig. 4. The Zn K-edge XANES in Fig. 4a shows that the x-ray absorption edge position of Zn-SAC is significantly different from bulk Zn, indicating that the valence state of Zn in Zn-SAC is different from Zn (0) in the bulk Zn phrase. Similarly, the XANES spectrum of Mo-SAC in Fig. 4b does not overlap with the Mo foil, implying a difference in metal oxidation state from the Mo-Mo closest packed metal structure. In addition, the coordination between metal and nitrogen were further studied using the EXAFS Fourier transform (FT) for Zn-SAC and Mo-SAC, displayed in Fig. 4c and d. The FT-EXAFS spectrum for Zn-SAC (Fig. 4c) shows a major peak at 1.49 Å, attributed to the Zn-N peak, while a distinct peak at 2.29 Å belonging to Zn-Zn bonds were present, verifying

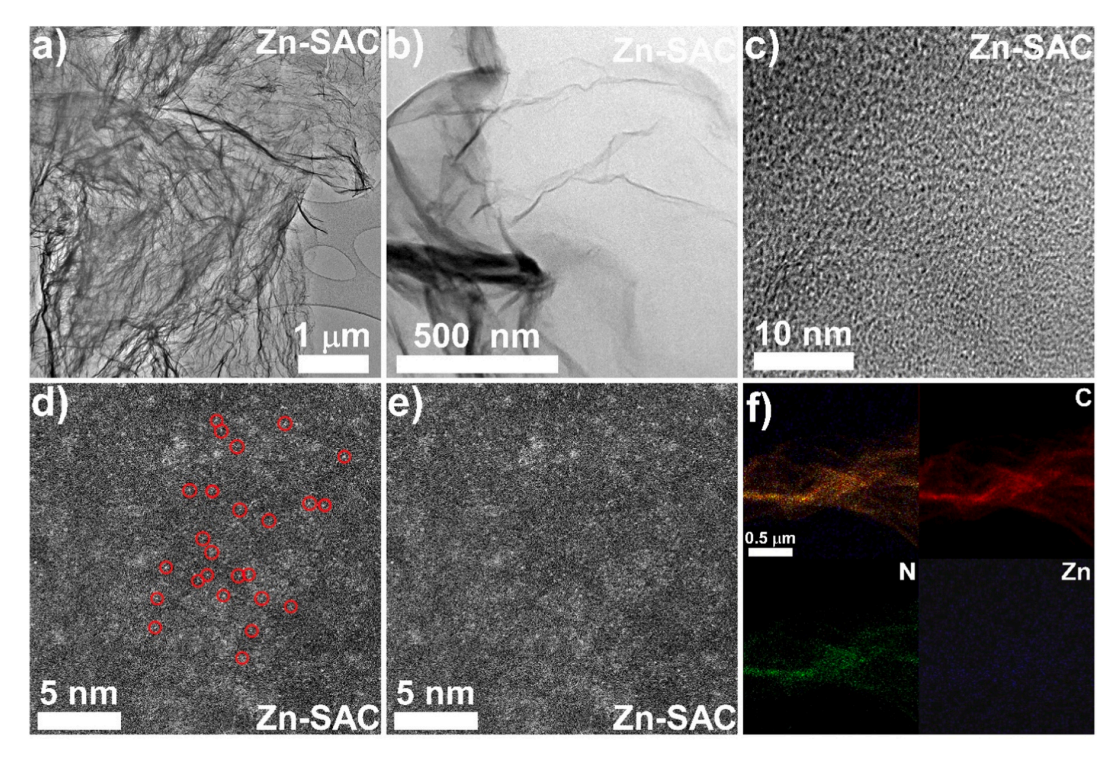


Fig. 3. Atomic and morphology characterization of Zn-SAC. (a) Low- and (b, c) high-resolution STEM image of Zn-SAC. (d, e) Zoom-in STEM image of Zn-SAC at high magnification (Zn single atoms are marked by red circles). (f) EDS mapping showing the homogenous distribution and presence of the elements of C, N and Zn in the Zn-SAC composite.

the coordination of Zn with N.[45,46]Similar results were obtained in the FT-EXAFS spectrum for Mo-SAC in Fig. 4d, with a dominant peak observed at 1.04 Å (Mo-N/C), quite different from the peak at 2.55 Å (Mo-Mo) observed in Mo foil curve, indicating Mo-N coordination in the Mo-SAC. [47,48].

The electrochemical properties of Zn-SAC for ORR/ OER were examined and compared with NG and Mo-SAC in LOBs. As compared with the CV tests in pure argon (Fig. S8a-c, Supporting Information), the CV curves with oxygen supply (Fig. S8d-f, Supporting Information) display a pair distinct oxidation and reduction peaks at around 3.2-3.4 and 2.2-2.5 V, respectively. Furthermore, the cathodic peak location of Zn-SAC is slightly more positive than that of Mo-SAC and pure graphene. indicating that the Zn-SAC had superior catalytic activity on ORR process. In addition, larger integration regions were found in Mo and Zn-SACs electrode, indicating the role of single atom catalyst. Fig. 5a shows the cell configuration in which our composite was cast onto carbon paper as cathode and assembled with separator and lithium anode. The overpotentials of NG, Mo-SAC and Zn-SAC were examined and tested with the designated capacity of 0.1 mAh cm⁻² at the current density of 0.05 mA cm^{-2} . Among the three samples, NG has the highest ORR overpotential of 0.22 V at the first discharge cycle. (Fig. 5b) The η_{ORR} increased along the cycling and reached 0.58 V after 50 cycles, accounting for 174% increase from the 1st cycle. In the charging process (OER), NG delivered a high OER overpotential of 1.32 V, due to the insulating nature of lithium peroxides, making the decomposition of Li₂O₂ difficult for subsequent oxidation, thus increasing the OER overpotential. Mo-SAC delivered a slightly reduced η_{ORR} of 0.19 V at first discharge cycle, but its catalytic activity decreased dramatically during cycling with η_{ORR} increased to 0.64 V after 50 cycles. (Fig. 5c), accounted for 232.4% change from the 1st cycle. In the OER process, Mo-SAC has 1.34 V reaction overpotential, which increased to 1.78 V after 50 cycles. In sharp contrast, Zn-SAC rendered a rather stable cyclability (Fig. $5\boldsymbol{d})$ that achieved the η_{ORR} of 0.20 V at the beginning

and retained the value 0.22 V after 30 cycles, achieving 0.07% overpotential retention rate. In addition, Zn-SAC delivered a η_{ORR} of 0.4 V after 50 cycles, a comparatively small increase in the overpotential, compared to NG and Mo-SAC. Similarly, after 50 cycles, Zn-SAC exhibited the smallest OER overpotential of 1.66 V, revealing the superior catalytic activity of Zn-SAC in ORR/OER process. Figs. 5e and 5f compare the discharge/ charge curves of NG, Mo-SAC and Zn-SAC at 1st and 50th cycle to verify the stability of the three samples. On the first cycle, a flat discharge plateau at 0.2 V was observed for both samples, while similar OER performances were found. After 50 cycles, Zn-SAC showed the best performance, retaining 0.4 and 1.66 V discharge and charge overpotential, respectively, while NG and Mo-SAC performance both deteriorated greatly during cycling. Interestingly, we found the similar trend that the Φ decrease with decreasing experimentally measured OER overpotential and the overpotential retention rate. Thus, our experimental electrochemical performances verify our calculation results, demonstrating the advantages of Zn-SAC in ameliorating overpotential and enhancing cycling durability in LOBs.

4. Summary and conclusion

In this work, we used the density functional theory (DFT) flavor of quantum mechanics to derive the SAC activity relationship with Gibbs free energy of LiO₂ to explore the origin of ORR/ OER activity in LOBs for a series of d-block metal. The calculated Gibbs free energy diagram helps understand the thermodynamics of the ORR/ OER process in LOBs. We found a linear correlation of reaction overpotentials with ΔG_{LiO_2} so that weak interaction between the SAC and LiO₂ reduces the overpotentials. Based on the DFT results, we developed a descriptor, Φ based on the intrinsic properties of the SAC metal in M-N₄ moieties on carbon scaffold with the help of trained machine learning (ML). Interestingly, we found that the catalytic activity $(\eta_{overall})$ is linearly correlated with the descriptor, providing guidance for designing efficient SACs for ORR/

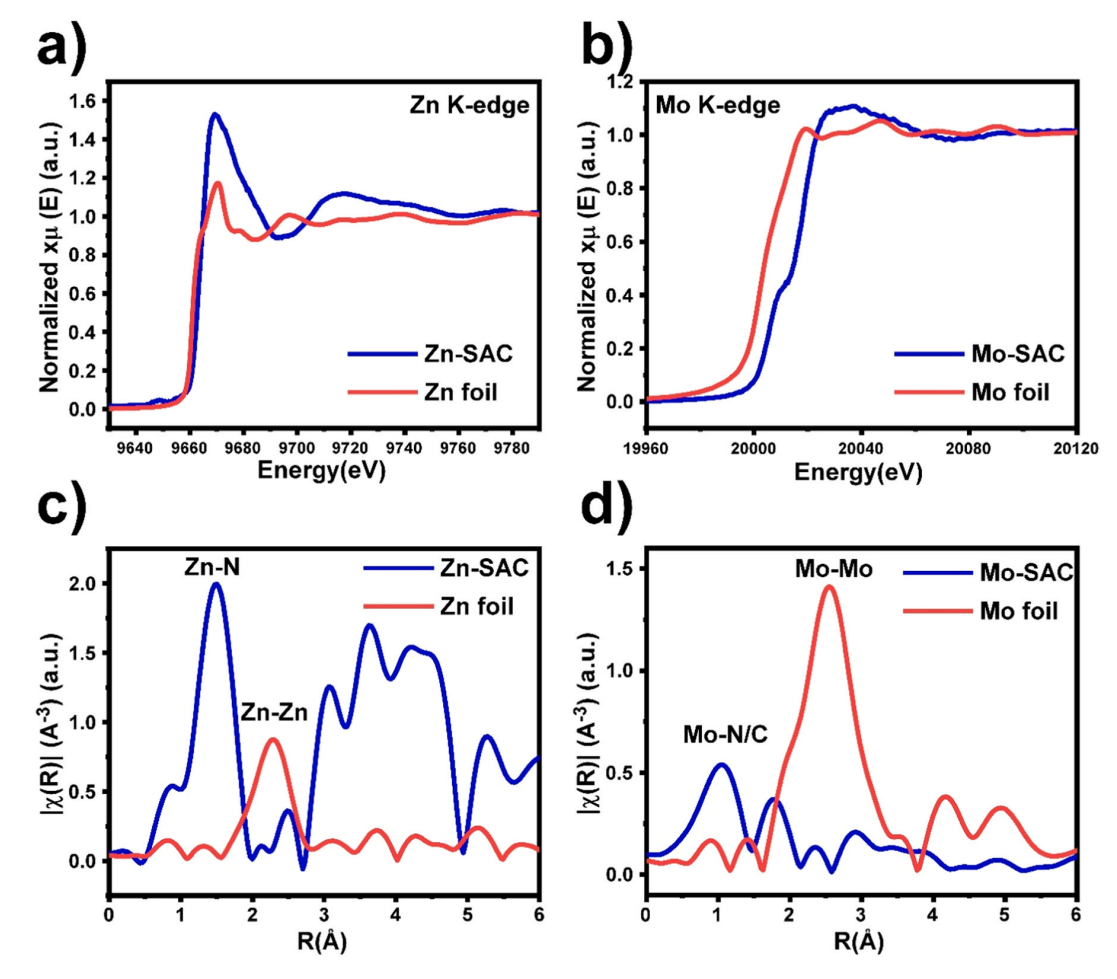


Fig. 4. Structural and chemical state characterization by X-ray absorption fine structure (XAFS) measurement. Normalized metal K-edge X-ray absorption near-edge structure (XANES) spectra for (a) Zn-SAC and (b) Mo-SAC. The corresponding Fourier transform (FT) magnitudes of EXAFS spectra in R space of (c) Zn-SAC and (d) Mo-SAC.

OER catalysis. This indicated high activity of Zn-SAC among all studied SACs. To verify our computational results, we synthesized two SACs (Zn and Mo) and characterized them experimentally. We confirmed the high loading and homogenous distribution of the single metal atom on N-doped graphene surface were confirmed by the ADF-STEM and XAFS characterizations. In addition, our electrochemical experiments show that Zn-SAC has significantly higher cycling stability over the Mo-SAC and NG with reduced discharge/ charge overpotentials. Our work provides guidelines for designing highly efficient SACs for catalyzing the ORR/ OER process in LOBs to support the development of high energy storage and conversion applications.

There are limitations and challenges in the synthesis and characterization of SACs. For example, traditional characterization methods like TEM and XRD are difficult to examine the structure of SACs to identify the metal atoms and the metal bonding. In terms of scalability of the synthesis process of SACs, challenges remain for scaling up the laboratory scale of the production process to the industrial level. Specifically, factors, like reaction kinetics, mass transport in the reactor and the cost considerations need to be addressed when developing industrial-scale synthesis process to ensure a cost effectiveness and high throughput without compromising the quality of the SACs. One possible solution to reduce the production cost is to identify abundant and low-cost precursors for the SACs synthesis.

CRediT authorship contribution statement

Cai Yuting: Visualization. Wang Jun: Data curation, Methodology, Writing – original draft. Hossain Md Delowar: Conceptualization, Data curation, Methodology, Supervision. Tang Tsz Wing: Data curation, Methodology, Writing – original draft, Writing – review & editing. Wong Hoilun: Conceptualization, Data curation, Methodology, Visualization, Writing – original draft, Writing – review & editing. Amine Khalil: Writing – review & editing. Liu Hongwei: Writing – review & editing. Liu Zhenjing: Writing – review & editing. Huang Xiaozhou. Data curation, Methodology, Writing – original draft. Tamtaji Mohsen: Data curation, Methodology, Writing – original draft. Liu Tongchao: Data curation, Methodology. Luo Zhengtang: Conceptualization, Funding acquisition, Supervision, Writing – review & editing. Goddard William A.: Conceptualization, Supervision, Writing – review & editing.

Declaration of Competing Interest

The authors declare that they have no known competing financial interests or personal relationships that could have appeared to influence the work reported in this paper.

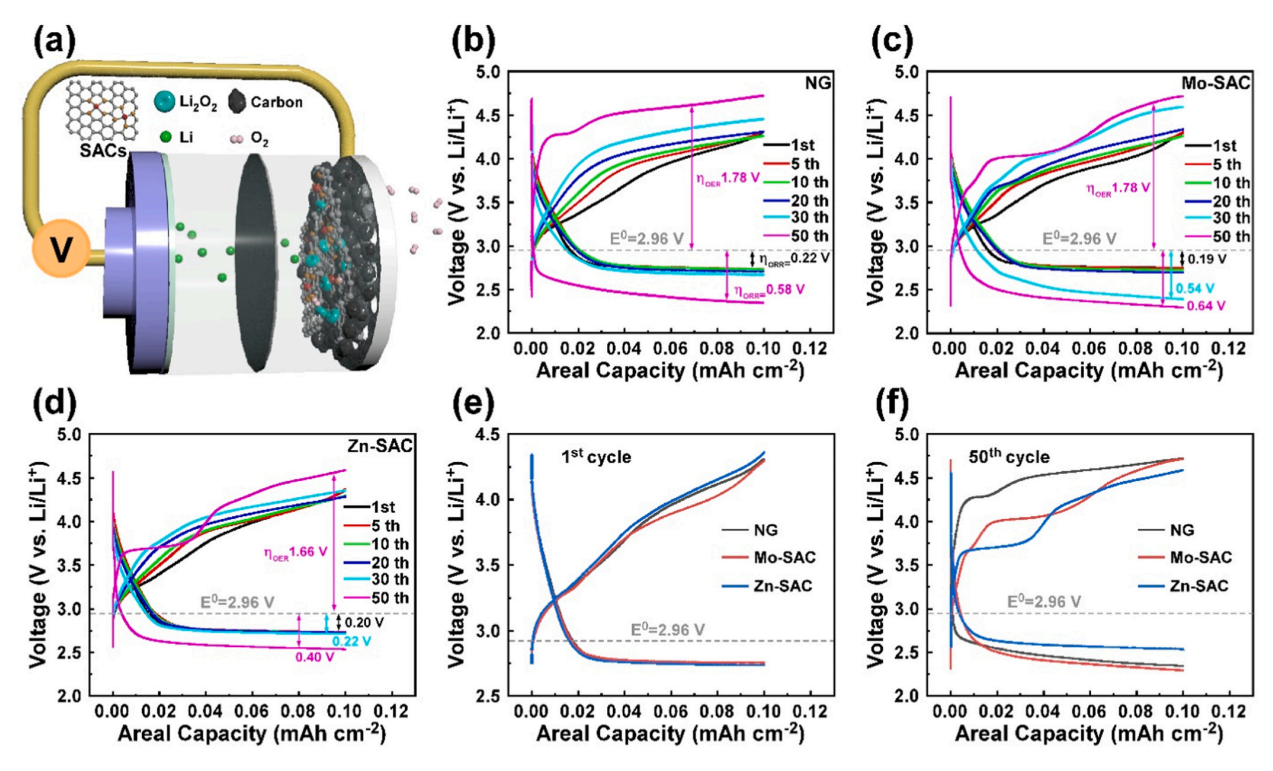


Fig. 5. Electrochemical performance of Zn-SAC, Mo-SAC, and NG. (a) Schematic illustration of the LOBs cell configuration model based on Zn-SAC cathode. The discharge-charge curves of (b) NG, (c) Mo-SAC and (d) Zn-SAC at a current density of 0.05 mA cm⁻² and areal capacity of 0.1 mAh cm⁻². Comparison of cell overpotential at (e) 1st and (f) 50th cycle, indicating retention of Zn-SAC activity after battery cycling.

Data availability

Data will be made available on request.

Acknowledgment

The work described in this paper was partially supported by a grant from the Research Grants Council of the Hong Kong Special Administrative Region, China (Project No. HKUST C6008-20E, 16304421), Research Fund of Guangdong-Hong Kong-Macao Joint Laboratory for Micro-Nano Optoelectronic Technology (2020B1212030010), and Shenzhen Special Fund for Central Guiding the Local Science and Technology Development (2021Szvup136). WAG received support from NSF US (CBET (2311117) and from the Hong Kong Quantum AI Lab, AIR@InnoHK of Hong Kong Government. This work gratefully acknowledges support from the U. S. Department of Energy (DOE), Office of Energy Efficiency and Renewable Energy, Vehicle Technologies Office. Argonne National Laboratory is operated for DOE Office of Science by UChicago Argonne, LLC, under contract number DE-AC02-06CH11357. Use of the National Synchrotron Light Source II (7-BM) is supported by the US Department of Energy, an Office of Science user Facility operated by Brookhaven National Laboratory under contract number DE-SC0012704. Technical support from the Advanced Engineering Materials Facilities and the Materials Characterization and Preparation Facilities at HKUST is greatly appreciated.

Appendix A. Supporting information

Supplementary data associated with this article can be found in the online version at doi:10.1016/j.nanoen.2024.109279.

References

- [1] W.J. Kwak, Rosy, D. Sharon, C. Xia, H. Kim, L.R. Johnson, P.G. Bruce, L.F. Nazar, Y. K. Sun, A.A. Frimer, M. Noked, S.A. Freunberger, D. Aurbach, Chem. Rev. 120 (2020) 6626-6683.
- M. Balaish, J.W. Jung, I.D. Kim, Y. Ein-Eli, Adv. Funct. Mater. 30 (2019).
 P. Zhang, M. Ding, X. Li, C. Li, Z. Li, L. Yin, Adv. Energy Mater. 10 (2020).
- [4] J.-W. Jung, S.-H. Cho, J.S. Nam, I.-D. Kim, Energy Storage Mater. 24 (2020)
- Y.-C. Lu, B.M. Gallant, D.G. Kwabi, J.R. Harding, R.R. Mitchell, M.S. Whittingham, Y. Shao-Horn, Energy Environ. Sci. (2013) 6.
- [6] F. Li, J. Chen, Adv. Energy Mater. 7 (2017).
- [7] D. Geng, N. Ding, T.S.A. Hor, S.W. Chien, Z. Liu, D. Wuu, X. Sun, Y. Zong, Adv. Energy Mater. 6 (2016).
- [8] G. Wu, N.H. Mack, W. Gao, S. Ma, R. Zhong, J. Han, J.K. Baldwin, P. Zelenay, ACS Nano 6 (2012) 9764-9776.
- [9] H. Kim, H. Lee, M. Kim, Y. Bae, W. Baek, K. Park, S. Park, T. Kim, H. Kwon, W. Choi, K. Kang, S. Kwon, D. Im, Carbon 117 (2017) 454-461.
- [10] S. Huang, W. Fan, X. Guo, F. Meng, X. Liu, ACS Appl. Mater. Interfaces 6 (2014) 21567-21575.
- [11] J. Xiao, D. Wang, W. Xu, D. Wang, R.E. Williford, J. Liu, J.-G. Zhang, J. Electrochem. Soc. 157 (2010).
- S.S. Zhang, D. Foster, J. Read, J. Power Sources 195 (2010) 1235–1240.
- [13] Z. Peng, S.A. Freunberger, Y. Chen, P.G. Bruce, Science 337 (2012) 563-566.
- H.-D. Lim, H. Song, H. Gwon, K.-Y. Park, J. Kim, Y. Bae, H. Kim, S.-K. Jung, T. Kim, Y.H. Kim, X. Lepró, R. Ovalle-Robles, R.H. Baughman, K. Kang, Energy Environ. Sci. 6 (2013) 3570.
- [15] F. Li, D.M. Tang, Y. Chen, D. Golberg, H. Kitaura, T. Zhang, A. Yamada, H. Zhou, Nano Lett. 13 (2013) 4702-4707.
- [16] X. Meng, K. Liao, J. Dai, X. Zou, S. She, W. Zhou, F. Ye, Z. Shao, ACS Appl. Mater. Interfaces 11 (2019) 20091–20097.
- Y.C. Lu, Z. Xu, H.A. Gasteiger, S. Chen, K. Hamad-Schifferli, Y. Shao-Horn, J. Am. Chem. Soc. 132 (2010) 12170-12171.
- [18] J.J. Xu, Z.W. Chang, Y.B. Yin, X.B. Zhang, ACS Cent. Sci. 3 (2017) 598-604.
- [19] P. Wang, C. Li, S. Dong, X. Ge, P. Zhang, X. Miao, R. Wang, Z. Zhang, L. Yin, Adv. Energy Mater. 9 (2019).
- [20] Y. Hou, J. Wang, J. Liu, C. Hou, Z. Xiu, Y. Fan, L. Zhao, Y. Zhai, H. Li, J. Zeng, X. Gao, S. Zhou, D. Li, Y. Li, F. Dang, K. Liang, P. Chen, C. Li, D. Zhao, B. Kong, Adv. Energy Mater. 9 (2019) 1901751.
- [21] J.-W. Jung, D.-W. Choi, C.K. Lee, K.R. Yoon, S. Yu, J.Y. Cheong, C. Kim, S.-H. Cho, J.-S. Park, Y.J. Park, I.-D. Kim, Nano Energy 46 (2018) 193–202.
- [22] Y.B. Yin, J.J. Xu, Q.C. Liu, X.B. Zhang, Adv. Mater. 28 (2016) 7494-7500.

[23] C. Xia, Y. Qiu, Y. Xia, P. Zhu, G. King, X. Zhang, Z. Wu, J.Y.T. Kim, D.A. Cullen, D. Zheng, P. Li, M. Shakouri, E. Heredia, P. Cui, H.N. Alshareef, Y. Hu, H. Wang, Nat. Chem. 13 (2021) 887-894.

[24] R. Gusmão, M. Veselý, Z. Sofer, ACS Catal. 10 (2020) 9634–9648.

- [25] B. Qiao, A. Wang, X. Yang, L.F. Allard, Z. Jiang, Y. Cui, J. Liu, J. Li, T. Zhang, Nat. Chem. 3 (2011) 634-641.
- [26] X.F. Yang, A. Wang, B. Qiao, J. Li, J. Liu, T. Zhang, Acc. Chem. Res 46 (2013) 1740-1748.
- [27] C.H. Choi, M. Kim, H.C. Kwon, S.J. Cho, S. Yun, H.T. Kim, K.J. Mayrhofer, H. Kim, M. Choi, Nat. Commun. 7 (2016) 10922.
- [28] J. Zhang, X. Wu, W.C. Cheong, W. Chen, R. Lin, J. Li, L. Zheng, W. Yan, L. Gu, C. Chen, Q. Peng, D. Wang, Y. Li, Nat. Commun. 9 (2018) 1002.
- [29] X. Hu, G. Luo, Q. Zhao, D. Wu, T. Yang, J. Wen, R. Wang, C. Xu, N. Hu, J. Am. Chem. Soc. 142 (2020) 16776-16786.
- [30] L.N. Song, W. Zhang, Y. Wang, X. Ge, L.C. Zou, H.F. Wang, X.X. Wang, Q.C. Liu, F. Li, J.J. Xu, Nat. Commun. 11 (2020) 2191.
- [31] P. Wang, Y. Ren, R. Wang, P. Zhang, M. Ding, C. Li, D. Zhao, Z. Qian, Z. Zhang, L. Zhang, L. Yin, Nat. Commun. 11 (2020) 1576.
- [32] X. Hu, G. Luo, Q. Zhao, D. Wu, T. Yang, J. Wen, R. Wang, C. Xu, N. Hu, J. Am. Chem. Soc. 142 (2020) 16776-16786.
- [33] J. Kang, J.S. Yu, B. Han, J. Phys. Chem. Lett. 7 (2016) 2803-2808.
- [34] H.R. Jiang, T.S. Zhao, L. Shi, P. Tan, L. An, J. Phys. Chem. C. 120 (2016) 6612-6618.
- [35] K.-H. Yun, Y. Hwang, Y.-C. Chung, J. Power Sources 277 (2015) 222–227.
 [36] M. Tamtaji, H. Gao, M.D. Hossain, P.R. Galligan, H. Wong, Z. Liu, H. Liu, Y. Cai, W. A. Goddard, Z. Luo, J. Mater. Chem. A 10 (2022) 15309-15331.
- [37] M. Tamtaji, X. Guo, A. Tyagi, P.R. Galligan, Z. Liu, A. Roxas, H. Liu, Y. Cai, H. Wong, L. Zeng, J. Xie, Y. Du, Z. Hu, D. Lu, W.A. Goddard 3rd, Y. Zhu, Z. Luo, ACS Appl. Mater. Interfaces 14 (2022) 46471-46480.
- [38] M. Tamtaji, S. Cai, W. Wu, T. Liu, Z. Li, H.-Y. Chang, P.R. Galligan, S.-i Iida, X. Li, F. Rehman, K. Amine, W.A. Goddard, Z. Luo, J. Mater. Chem. A 11 (2023) 7513–7525.
- [39] M.D. Hossain, Z. Liu, M. Zhuang, X. Yan, G.L. Xu, C.A. Gadre, A. Tyagi, I.H. Abidi, C.J. Sun, H. Wong, A. Guda, Y. Hao, X. Pan, K. Amine, Z. Luo, Adv. Energy Mater. 9 (2019).
- [40] M. Tamtaji, Q. Peng, T. Liu, X. Zhao, Z. Xu, P.R. Galligan, M.D. Hossain, Z. Liu, H. Wong, H. Liu, K. Amine, Y. Zhu, W.A. Goddard Iii, W. Wu, Z. Luo, Nano Energy 108 (2023).
- [41] H. Wong, X. Ou, M. Zhuang, Z. Liu, M.D. Hossain, Y. Cai, H. Liu, H. Lee, C.Z. Wang, Z. Luo, ACS Appl. Mater. Interfaces 11 (2019) 19986–19993.
- [42] Y. Li, H. Wong, J. Wang, W. Peng, Y. Shen, M. Xu, Q. An, J.K. Kim, B. Yuan, W. A. Goddard, Z. Luo, Adv. Energy Mater. 12 (2022).
- [43] F. Yang, P. Song, X. Liu, B. Mei, W. Xing, Z. Jiang, L. Gu, W. Xu, Angew. Chem. 57 (2018) 12303–12307.
- [44] L. Han, X. Liu, J. Chen, R. Lin, H. Liu, F. Lü, S. Bak, Z. Liang, S. Zhao, E. Stavitski, J. Luo, R.R. Adzic, H.L. Xin, Angew. Chem. 131 (2019) 2343-2347.
- [45] Z. Zhao, H. Tan, P. Zhang, X. Liang, T. Li, Y. Gao, C. Hu, Angew. Chem. 62 (2023) e202219178
- [46] H. Yang, L. Shang, Q. Zhang, R. Shi, G.I.N. Waterhouse, L. Gu, T. Zhang, Nat. Commun. 10 (2019) 4585.
- [47] Y. Wang, G. Jia, X. Cui, X. Zhao, Q. Zhang, L. Gu, L. Zheng, L.H. Li, Q. Wu, D. J. Singh, D. Matsumura, T. Tsuji, Y.-T. Cui, J. Zhao, W. Zheng, Chem 7 (2021) 436-449
- [48] W. Chen, J. Pei, C.T. He, J. Wan, H. Ren, Y. Zhu, Y. Wang, J. Dong, S. Tian, W. C. Cheong, S. Lu, L. Zheng, X. Zheng, W. Yan, Z. Zhuang, C. Chen, Q. Peng, D. Wang, Y. Li, Angew. Chem. 56 (2017) 16086-16090.



Hoilun Wong received her Ph.D. in Chemical and Biological Engineering from the Hong Kong University of Science and Technology in 2023. Her research interest is focusing on the fundamental study on electronic properties of 2D nanomaterials for applications of high energy metal batteries using DFT calculations.



Dr. Tongchao Liu currently works as an Assistant Chemist at Argonne National Laboratory. He obtained his Ph.D. degree from Peking University in 2019. His research interests focus on electrochemical energy storage, battery materials, and materials characterization, in particular, fundamental understanding of failure chemistries through in-situ synchrotron-based Xray techniques.



Mohsen Tamtaji received his PhD in Chemical and Biological Engineering from the Hong Kong University of Science and Technology in 2022. He is currently a postdoctoral fellow at the Hong Kong Quantum AI lab (HKQAI). His research interest focuses on the application of Machine Learning (ML) and DFT calculations on the rational design of photo- and electrocatalysts.



Xiaozhou Huang earned his Ph.D. from the mechanical engineering department at George Mason University, specializing in research areas such as catalysts for lithium oxygen battery. solid state battery, generation of reactive oxygen species, and chemical sensors



Tsz Wing Tang is a PhD candidate in Chemical and Biological Engineering at the Hong Kong University of Science and Technology. Her research primarily focuses on defect engineering in two dimensional (2D) materials, specifically hexboron nitride (hBN) and transitional metal dichalcogenides (TMDs) utilizing chemical vapor deposition (CVD), and the applications of these materials in the fields of photonics and electronics.



Md Delowar Hossain is currently working as a Postdoctoral Fellow at SUNCAT Center for Interface Science and Catalysis under the Department of Chemical Engineering, Stanford University, and SLAC. He received his Ph.D. in Chemical and Biological Engineering from the Hong Kong University of Science and Technology in 2020. My current research focus consists of the computational design of highly active, stable, lowcost heterogeneous catalysts for various electrochemical conversion reactions.



Jun Wang is now a PhD student supervised by Prof. Zhengtang LUO in the Hong Kong University of Science and Technology. His current research interest focuses on optical properties of two-dimensional layered materials.



Dr. Khalil Amine is an Argonne Distinguished Fellow and the leader of the Advanced Battery Technology team at Argonne National Laboratory. He currently serves as a committee member of the U.S. National Research Consul, US Academy of Sciences on battery related technologies. He is an adjunct distinguished professor at Stanford University and hold a joint appointment as professor at the university of Chicago. Among his many awards, Dr. Amine is the 2019 reception of the prestigious Global Energy Prize. He is also six-time recipient of the R&D 100 Award, which is considered as the Oscar of technology and innovation. He is an ECS fellow, and associate editor of the journal of Nano-Energy.



Yuting Cai is currently a postdoctoral researcher at The Hong Kong University of Science and Technology. He received his B. Sc. degree in Material Science and Engineering from Sichuan University in 2017. He then pursued and received his Ph.D. degree in Chemical and Biomolecular Engineering from the Hong Kong University of Science and Technology in 2021. His research interests focus mainly on 2D materials for wearable electronics and biomedical applications.

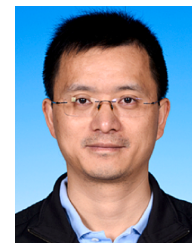


William A. Goddard III is the Charles and Mary Ferkel Professor of Chemistry and Applied Physics, and Director, Materials and Process Simulation Center at the California Institute of Technology He obtained his B.S. Engineering (highest honors) from the University of California, Los Angeles, in 1960 and his Ph.D. in Engineering Science (minor physics) from the California Institute of Technology, 1965. He joined the Chemistry faculty at Caltech in November 1964. He was elected to the National. Academy of Science US in 1984. He has published over 1580 papers (H index = 187, I-10 index 1350) and been issued 29 Patents (15 pending). He was named #17 international (#12 US) Best Chemistry Scientists by Research.com (https://research.com/scientists-rankings/chemistry) based

on D-index (chemistry only). Goddard has been and continues to be a pioneer in developing methods for quantum mechanics (QM), force fields (FF), and reactive dynamics (RD) and the applications of these methods to design new materials for improving homogeneous and heterogeneous catalysis, electrocatalysis, batteries, fuel cells, energetic materials, and pharma. A recent advance is Grand Canonical QM to describe electrochemical reactions at constant applied potential (rather than constant electrons). The goal of the Goddard research is to make the methods sufficiently accurate that the need for experimental validation can be severely restricted to the predicted very best systems.



Zhenjing Liu got her B.S. degree in materials science and engineering from Shanghai Jiao Tong University, and Ph.D. degree in chemical and biological engineering from the Hong Kong University of Science and Technology. Her research focused on the controlled synthesis of 2D materials via chemical vapor deposition method towards energy application.



Prof. Zhengtang Luo is currently a professor with tenure at the Hong Kong University of Science and Technology. He obtained his bachelor's degree from South China University of Technology and his PhD degree (in Polymer Science) from University of Connecticut, followed by postdoctoral training (in Physics) at University of Pennsylvania. His research focus on materials chemistry and physics, and product development for applications in chemical industry.



Hongwei Liu received his PhD in chemical and biological engineering from Hong Kong University of Science and Technology in 2023. His research focuses on the controllable synthesis of two-dimensional materials including graphene, hexagonal boron nitride and transition metal dichalcogenides by chemical vapor deposition.